ISSN: 2476-6909; Modares. Mech. Eng. *2026;26(09):707-724.*

Modares Mechanical Engineering

DOI: 10.48311/mme.2025.96920.0

journal homepage: www.mme.modares.ac.ir

On Multi-Criteria Optimization of DVAs in Vibration Control of 2-DOF Systems: Parsimonious FRF Shaping of DVAs via a Singular Criterion and Genetic Algorithm Optimization

Mahan Dashti Gohari, Mehdi Mohammadimehr*

Faculty of Mechanical Engineering, University of Kashan

ARTICLE INFO

Article Type
Original Research

Article History
Received: August 23, 2025
Revised: November 03, 2025
Accepted: November 24, 2025
ePublished: June 20, 2026

ABSTRACT

Conventional DVA optimization offers little direct control over shaping the frequency response, and weak parameter screening lets unnecessary variables persist, leading to over-parameterized designs. This paper presents a unique criterion (C_s) that integrates normalized, weighted objectives for peak positions, peak amplitudes, bandwidth, and other factors, incorporating a specific sparsity term that mitigates the inclusion of superfluous parameters. The framework is implemented in the DeVana software, which was developed by the authors, and it is utilized for a fully coupled 1DOF–1DOF benchmark that includes a designated avoidance band within the frequency range of 1000 to 2000 Hz for the purpose of conducting a case study. The optimized DVA divides the baseline resonance into two narrow peaks at the band edges and attenuates the in-band response, while the majority of ν parameters approach zero, leaving only a limited set of β, λ, and μ active. Convergence was achieved at an optimal fitness of 0.001206. This fitness is composed of 40.8% from C_s, 34.7% from the sparsity penalty, and 24.5% from the target-accuracy term. Overall, combining the design goals into a single, interpretable objective enables direct FRF targeting and streamlined DVA synthesis, delivering rapid, criteria-satisfying tuning with only the minimal set of screened parameters.

Keywords: Dynamic vibration absorber, Vibration control, Frequency response function shaping, Singular criterion, Multi criteria optimization

How to cite this article
Dashti Gohari M, Mohammadimehr M, On Multi-Criteria Optimization of DVAs in Vibration Control of 2-DOF Systems: Parsimonious FRF Shaping of DVAs via a Singular Criterion and Genetic Algorithm Optimization. Modares Mechanical Engineering; *2026;26(09):707-724.*

**Corresponding author's email: mmohammadimehr@kashanu.ac.ir*
**Corresponding ORCID ID: 0000-0002-2975-4514*

شاپا: ۶۹۰۹-۲۴۷۶؛ مهندسی مکانیک مدرس. ۷۲۴-۷۰۷:(۰۹)۲۶;۱۴۰۵

مهندسی مکانیک مدرس

DOI: 10.48311/mme.2025.96920.0

صفحه اصلی مجله: mme.modares.ac.ir

بهینه‌سازی چندمعیاره جاذب‌های دینامیکی ارتعاشات (DVA) در کنترل ارتعاش سامانه‌های دو درجه‌آزادی: شکل‌دهی بهینه و کم‌پارامتر تابع پاسخ فرکانسی جاذب‌های دینامیکی ارتعاشات با استفاده از یک معیار تکین و بهینه‌سازی به کمک الگوریتم ژنتیک

ماهان دشتی گوهری، مهدی محمدی مهر*

دانشکده مهندسی مکانیک، دانشگاه کاشان

اطلاعات مقاله

نوع مقاله

مقاله پژوهشی

تاریخچه مقاله

دریافت: ۱۴۰۴/۰۶/۰۱

بازنگری: ۱۴۰۴/۰۸/۱۲

پذیرش: ۱۴۰۴/۰۹/۰۳

ارائه آنلاین: ۱۴۰۵/۰۳/۳۰

چکیده

روش های بهینه سازی متداول جاذب های دینامیکی ارتعاشات (DVA) کنترل مستقیم کمی روی شکل دهی پاسخ فرکانسی دارند. از طرف دیگر، چون غربالگری پارامترها ضعیف است، متغیرهای غیرضروری حذف نمی شوند و در نتیجه طراحی ها با تعداد پارامترهای زیاد شکل می گیرند. در این مقاله، یک معیار منحصر به فرد به نام (C_s) معرفی می شود که چند هدف نرمال سازی شده و وزن دهی شده را در یک معیار واحد جمع می کند؛ از جمله هدف های مربوط به محل قله ها، دامنه قله ها، پهنای باند می توان اشاره کرد. علاوه بر این، یک جمله مشخص تنکی (sparsity) هم در این معیار قرار داده شده است تا از اضافه شدن پارامترهای زائد جلوگیری کند. این چارچوب در نرم افزار DeVana پیاده سازی شده است؛ نرم افزاری که نویسندگان آن را توسعه داده اند. سپس برای انجام یک مطالعه موردی، از یک مساله مرجع کاملا کوپل شده تک درجه آزادی – تک درجه آزادی استفاده شده است که در آن یک باند اجتناب مشخص در محدوده فرکانسی ۱۰۰۰ تا ۲۰۰۰ Hz در نظر گرفته می شود. نتایج نشان می دهد جاذب دینامیکی بهینه شده، رزونانس مبنا را به دو قله باریک در دو لبه باند تبدیل می کند و پاسخ داخل باند را کاهش می دهد. همزمان، بیشتر پارامترهای ν به سمت صفر می روند و فقط تعداد محدودی از پارامترهای β، λ و μ فعال باقی می مانند. همگرایی در مقدار برازش بهینه ۰/۰۰۱۲۰۶ به دست آمده است. این مقدار برازش از ۴۰/۸٪ مربوط به C_s، ۳۴/۷٪ مربوط به جریمه تنکی، و ۲۴/۵٪ مربوط به جمله دقت هدف تشکیل می شود. در مجموع، وقتی اهداف طراحی در قالب یک هدف واحد و قابل فهم ترکیب شوند، می توان FRF را به طور مستقیم هدف گذاری کرد و فرایند طراحی DVA را ساده تر انجام داد. نتیجه این کار، تنظیم سریع و مطابق معیارهای طراحی است، آن هم با حداقل مجموعه پارامترهایی که پس از غربالگری واقعا لازم هستند.

کلیدواژه‌ها: جاذب دینامیکی ارتعاشات، کنترل ارتعاش، شکل‌دهی تابع پاسخ فرکانسی، معیار تکین، بهینه‌سازی چندمعیاره.

نحوه ارجاع به این مقاله

دشتی گوهری ماهان، محمدی مهر مهدی، بهینه‌سازی چندمعیاره جاذب‌های دینامیکی ارتعاشات (DVA) در کنترل ارتعاش سامانه‌های دو درجه‌آزادی: شکل‌دهی بهینه و کم‌پارامتر تابع پاسخ فرکانسی جاذب‌های دینامیکی ارتعاشات با استفاده از یک معیار تکین و بهینه‌سازی به کمک الگوریتم ژنتیک ، مهندسی مکانیک مدرس. ۷۲۴-۷۰۷:(۰۹)۲۶;۱۴۰۵

*پست الکترونیکی نویسنده عهده‌دار مکاتبات: mmohammadimehr@kashanu.ac.ir

*شناسه ارکید نویسنده عهده‌دار مکاتبات: 0000-0002-2975-4514

Introduction

Dynamic vibration absorbers (DVAs) have a history that spans over a century. The concept originated by Frahm, who introduced a tuned absorber to reduce ship roll [1]. A more systematic theoretical foundation was established by Ormondroyd and Den Hartog, who analyzed undamped single-degree-of-freedom (SDOF) primary systems [2]. Den Hartog's subsequent work [3], along with later studies by Randall et al. [4] and Warburton [5], produced widely used closed-form tuning rules for linear absorbers under harmonic excitation.

The optimization DVAs represents a cornerstone of modern vibration control engineering, where the simultaneous tuning of multiple parameters including mass ratios, stiffness ratios, damping coefficients, and frequency relationships determines system effectiveness. Recent advances have shifted from traditional analytical methods toward sophisticated metaheuristic algorithms and hybrid approaches that can handle complex multi-objective optimization problems.

Gao et al. [6] combined fixed-point theory with particle swarm optimization (PSO) for optimizing three-element DVAs with inerter and negative stiffness elements, achieving improved parameter tuning and vibration control compared to using fixed-point theory alone. Chen et al. [7] extended the idea by employing intelligent algorithms to optimize multi-parameter Maxwell-type DVAs with inerter and negative stiffness elements. Their study revealed that the analytical and numerical solutions are consistent and effective. Zamani et al. [8] introduced a multi-objective optimization framework for double-tuned mass dampers (DTMD), utilizing seven metaheuristic algorithms and Pareto front analysis to achieve substantially improved vibration reduction and offer a wide range of optimal design solutions. Liu and Cheng [9] developed a fast univariate polynomial method for exact H_∞ DVA optimization, showing that equal resonant peak heights do not always ensure global optimality.

The integration of artificial intelligence (AI) and machine learning (ML) techniques into the field of dynamic vibration absorber (DVA) design has opened new avenues for both performance optimization and real-time control. Recent years have witnessed a growing trend towards leveraging data-driven models, physics-informed neural networks, and AI-assisted algorithms to achieve rapid, adaptive, and highly efficient solutions for vibration mitigation challenges. Tollardo et al. [10] introduced DeepF-fNet, a physics-informed neural network that rapidly optimizes vibration absorber parameters, outperforming traditional methods and paving the way for real-time vibration control.

Innovative DVA architectures and structural configurations have emerged in recent years, revealing new mechanisms for vibration mitigation and expanding application potential. Recent advances in triple-magnet magnetic dynamic vibration absorbers (TMDVAs) have introduced tunable stiffness through adjustable magnet distances, enabling effective optimization of vibration reduction under varying resonance conditions. Theoretical modeling frameworks established by Chen et al. [11] provided foundational equations for magnetic force interactions and system dynamics, facilitating design optimization.

Recent studies have advanced lever-based and amplification mechanisms in DVA design. Li et al. [12] showed that combining lever, inerter, and grounded stiffness in a Maxwell dynamic vibration absorber can yield superior vibration absorption when both viscoelastic and grounded stiffness components are positive. Recent advances in DVA research address uncertainty and robustness, with reliability-based and stochastic optimization emerging as key themes for resilient vibration control system design. Peng and Sun [13] applied reliability-based design optimization (RBDO) to tuned mass-damper-inerter (TMDI) systems for efficient vibration mitigation.

DVAs have recently been adopted across diverse engineering fields, including piping, aerospace, automotive, and civil structures, where advances in design and control have improved vibration suppression and system performance. Xing et al. [14] showed that combining linear DVAs with quasi-zero-stiffness systems improves low-frequency vibration isolation through parameter optimization. Chen et al. [15] used particle swarm optimization and time domain auto-tuning to efficiently design and prototype passive vibration absorbers for ropeway carrier systems. Athifah et al. [16] conducted experimental analysis of vibration reduction of boring bars with tapered mass-rubber dynamic vibration absorbers (MR-DVA). The research validated theoretical predictions through comprehensive experimental testing in machining applications. Shahraki et al. [17] investigated damage-based design of multiple tuned mass dampers to improve seismic performance of steel frame structures. The research introduced damage-based optimization criteria that considered structural damage as objective functions, providing more realistic TMD design for seismic protection. Besharatian et al. [18] studied particle swarm optimization of friction tuned mass dampers subjected to ground motion records. The research addressed design of TMDs with friction damping under seismic excitation, demonstrating advantages of PSO in handling nonlinear friction behavior. Mazloom et al. [19] studied a novel semiactive rolling tuned mass damper (SARTMD) that couples translational and rotational motions via a variable-inertia "umbrella" mechanism and a planetary gearbox to enable real-time frequency tuning and achieve large vibration suppression with a substantially reduced absorber mass compared to conventional TMDs. Mousaviyan Safakhaneh et al. [20] investigated a 10-story benchmark building with a rooftop active tuned mass damper (ATMD), proposing a response- and stiffness-based control algorithm that, under earthquake excitation, outperformed LQR and fuzzy-logic controllers by reducing average structural displacement and acceleration by 40% and 28.16%, respectively. Djerouni et al. [21] examined vibration mitigation for adjacent buildings using multiple tuned mass

dampers (MTMDs) configured either at the roof or distributed along the height and, using a hybrid PSO–GWO optimizer to tune mass, damping, and stiffness, showed across 462 earthquake records that distributed MTMDs most effectively reduce drift, pounding distance, and base shear, albeit with increased stroke demand in one non-rooftop device when compared with single TMDs and roof-only MTMDs. Advances in the analytical treatment of DVA design have played a crucial role in expanding the field's theoretical and practical foundations. Luo et al. [22] presented analytical optimization of the rotational inertia double tuned mass damper for structures under random excitation. Petrini et al. [23] studied optimal tuned mass-damper-inerter (TMDI) design in wind-excited tall buildings for occupants' comfort serviceability performance and energy harvesting. Integration of energy harvesting technologies with dynamic vibration absorbers (DVAs) has gained significant momentum in recent years, enabling the simultaneous mitigation of unwanted vibrations and conversion of mechanical energy into usable electrical power. Contemporary DVA research has focused on the development of multi-functional devices in which vibration suppression and energy harvesting are not treated as competing objectives but rather as complementary aims.

With a lumped parallel configuration with two parallel absorbers, Jabbar et al. [24] improved dynamic vibration absorbers (DVAs) for structure vibration attenuation using negative mass and stiffness principles In the proposed model, stiffness, mass, and damping parameters decrease resonance amplitude and expand the frequency stopband. The best parameters are chosen by Nelder-Mead optimization. The average vibration amplitude decreased 91.46% in all three modes, and optimal selection reduced it 97.06%. The lumped parallel architecture with precisely adjusted negative mass and stiffness reduces vibration in many applications. Shamseldin et al. [25] propose four novel DVAs using hydraulic amplifiers (HA) to overcome lever mechanism limitations, mechanical inerters to improve vibration damping, and PSO and GA for multi-objective optimization. Artificial neural networks (ANNs) predict optimal hydraulic amplifier parameters and reduce friction loss to 10% of applied force. Mechanical inerters dampen vibrations. The research shows that HA and mechanical inerters improve vibration attenuation and frequency response, and PSO outperforms GA in solution diversity and quality. This integration may be useful in engineering. To improve vehicle dynamic performance due to nonpneumatic wheels' increased mass and vertical stiffness, Phuc and Hoang [26] developed a dynamic vibration damping system (NVDS). To study how increased wheel mass and stiffness affect vehicle dynamic performance, a quarter-vehicle model with the NPW's effective vertical stiffness is created. The multiobjective genetic algorithm is used to determine the optimal NVDS parameters for handling performance and ride comfort sensitivities. Results under different road excitations show that the proposed NVDS can significantly improve handling performance and ride comfort of vehicles with NPWs.

Despite significant advances in vibration absorber design, a number of critical limitations remain. Most existing methods rely on fixed, scalar performance metrics, without offering direct control over specific features of the frequency response function (FRF). As a result, engineers cannot easily prescribe the exact location of peaks, shape of attenuation zones, or bandwidth of vibration suppression. This makes it difficult to tailor absorber performance to specific application needs. Moreover, many tuning methods overlook practical constraints and often treat design objectives as static. Additionally, conventional optimization approaches typically use fixed algorithm parameters, which can lead to premature convergence or inefficient searches in complex, nonconvex design spaces. Furthermore, while evolutionary algorithms like genetic algorithms are widely used for absorber optimization, very few studies have implemented adaptive GA strategies, those that adjust mutation and crossover rates dynamically during the search. Existing works tend to apply fixed GA configurations or hybrid methods without systematically leveraging adaptive mechanisms specific to absorber design.

A central limitation in current practice is identified: “the absence of a tunable scalar design criterion that permits direct shaping of the FRF, together with the lack of a self-adaptive optimization framework that efficiently explores complex design spaces.” To address this limitation, the Singular Criterion (C_s) is proposed as a flexible objective that affords explicit control over FRF features, including peak positions and suppression bandwidth, while a sparsity term is incorporated to penalize redundant absorbers and tuning variables, thereby preventing overuse of DVAs. The methodology is implemented in **DeVana [27]**, where modeling, optimization, and analysis are integrated in a cohesive and open source program.

This paper introduces a new paradigm in DVA design through three key innovations. First, it proposes a single, tunable construct, the singular criterion (SC), that, for the first time, represents complex FRF targets in a compact scalar form. This unified metric enables direct and simultaneous control over peak positions, magnitudes, and bandwidths in absorber tuning. Second, the design framework embraces parsimony by embedding an explicit sparsity penalty, inherently steering the optimization toward minimal, efficient configurations and eliminating redundant absorber components and tuning variables. Third, the entire methodology is operationalized within a newly developed platform, DeVana, which integrates modeling, analysis, and adaptive optimization. DeVana leverages a self-adjusting genetic algorithm that dynamically refines its operators during the search, drastically improving robustness and convergence efficiency. The remainder of the paper is organized as follows. The methodology and the C_s formulation are introduced, including normalization and weighting of performance measures and the role of sparsity. The software implementation in DeVana is then summarized, followed by the optimization procedure and fitness composition. A fully coupled 1DOF-1DOF benchmark system is defined to provide a rigorous test bed. The results and discussion examine FRF shaping, fitness evolution, and parameter-wise convergence with emphasis on preventing unnecessary DVA use.

Methodology

Singular Criterion

The design of DVAs involves selecting appropriate combinations of mechanical components, including masses, springs, dampers, and inerters, to attach to a primary system for vibration reduction.

Let:

- $\mathcal{M} = \{m_i \mid m_i \in [m_i^{min}, m_i^{max}],\ i = 1, \dots, n_m\}$ Be a set of mass elements.
- $\mathcal{K} = \{k_j \mid k_j \in [k_j^{min}, k_j^{max}],\ j = 1, \dots, n_k\}$ Be a set of spring elements.
- $\mathcal{C} = \{c_l \mid c_l \in [c_l^{min}, c_l^{max}], l = 1, \dots, n_c\}$ Be a set of damping elements.
- $\mathcal{B} = \{b_p \mid b_p \in [b_p^{min}, b_p^{max}],\ p = 1, \dots, n_b\}$ Be a set of inerters

The placement of each element is categorized into either a continuous or discrete range, contingent upon the designer's capacity to utilize it within the viable and attainable design space. The overall quantity of potential configurations N_{config} is ascertained by the permutations of components:

$$N_{\text{config}} = (n_m + n_k + n_c + n_b)! \tag{1}$$

This factorial growth emphasizes how computational constraints make it impractical to thoroughly assess every potential configuration. For a given configuration S, the parameter vector $\boldsymbol{\theta_S}$ comprises the design variables associated with the included components:

$$\boldsymbol{\theta}_S = [\theta_1, \theta_2, \dots, \theta_{n_s}]^{\mathsf{T}} \tag{2}$$

where n_s is the number of parameters in configuration S, and each θ_i corresponds to a component parameter (e.g., mass, stiffness, damping coefficient, or inertance) within its viable range:

$$\theta_i \in [\theta_i^{min}, \theta_i^{max}] \tag{3}$$

The feasible parameter space for the configuration S can be then written as:

$$\Theta_s = \prod_{i=1}^{n_s} [\theta_i^{\min}, \theta_i^{\max}] \tag{4}$$

In the design of DVAs, various performance criteria must be met simultaneously to ensure effective vibration reduction, structural integrity, and operational efficiency. Let $\mathcal{C} = \{C_1, C_2, \dots, C_M\}$ represent the collection of performance criteria pertinent to DVA design. Each criterion C_i is associated with a target value T_i that reflects the desired performance level for that specific aspect. The target values T_i are determined based on engineering requirements, industry standards, or specific application needs. The relationship between each criterion and its target value is critical for ensuring that the optimized DVA meets the intended performance specifications.

To facilitate the optimization process, each performance criterion is normalized by its corresponding target value. The normalized criterion $\widetilde{C}_i(\boldsymbol{\theta})$ is defined as:

$$\widetilde{C}_i(\boldsymbol{\theta}) = \frac{C_i(\boldsymbol{\theta})}{T_i} \tag{5}$$

Multiple objectives can be combined into a single, singular criterion thanks to this normalization, which guarantees that all criteria are dimensionless and comparable. To facilitate optimization across multiple criteria, a singular criterion $C_s(\boldsymbol{\theta})$ is formulated as:

$$C_s(\boldsymbol{\theta}) = \sum_{i=1}^{M} w_i \widetilde{C}_i(\boldsymbol{\theta}) \tag{6}$$

$$\sum_{i=1}^{M} w_i = 1, \quad w_i \geq 0 \quad \forall i \tag{7}$$

Where $\widetilde{C}_i(\boldsymbol{\theta})$ is the normalized i-th performance criterion and the w_i is the weighting factor for the i-th criterion. The singularized criterion $C_s(\boldsymbol{\theta})$ serves as a unified metric encapsulating multiple performance objectives of the DVA design. The optimal value of C_s is achieved when:

$$C_s(\boldsymbol{\theta}^*) = 1 \tag{8}$$

This condition signifies that each normalized performance criterion meets its respective target value simultaneously.

In this research, the singular criterion $C_s(\theta)$ is defined as a weighted sum of normalized performance measures (Eqs. (5)–(7)). Each raw performance measure $C_i(\theta)$(for example, peak amplitude, peak location, bandwidth, etc.) is divided by its target value T_i, and the resulting normalized terms $\tilde{C}_i(\theta) = C_i(\theta)/T_i$ are combined with nonnegative weights w_i, where the weights are constrained to satisfy $\sum_i w_i = 1$. This construction makes $C_s$scale-free in two important senses:

1. **Unit independence:** Because each objective is normalized by its own target, all terms are dimensionless and comparable in magnitude. That means adding a new objective with different physical units (e.g. Hz vs. displacement amplitude) does not distort the scale of C_s.

2. **Objective-count independence:** Because the weights are normalized to sum to 1, the numerical range and interpretation of $C_s$do not "blow up" as the number of objectives increases. Even if more design criteria are appended, the contribution of each new criterion is explicitly controlled by its weight. In other words, $C_s = 1$still means "the FRF meets all specified targets," regardless of how many targets are being enforced, as stated in Eq. (8).

This is what we mean by the scalability of C_s: the same scalar score can still be used to drive optimization when you move from a simple tuning problem (e.g. match peak amplitude only) to a rich specification (e.g. simultaneously enforce two peak locations, suppress in-band amplitudes, and enforce a bandwidth requirement). The scalar objective remains interpretable and comparable across problem sizes, because every added criterion is just another normalized, weighted term in the same sum. In practice, this also lets the designer "dial in" priorities via w_i without having to redesign the optimization architecture.

Software Implementation: *DeVana* Program

The optimization framework used in this work is implemented in ***"DeVana"*** [27] an open-source software environment developed by the authors for the systematic design, tuning, and assessment of DVAs in multi-degree-of-freedom (MDOF) structures. DeVana is publicly available in full on GitHub, and the exact version used for this study is V0.6.2. This makes the methodology in this paper fully reproducible: all core functionality used here, model construction, frequency response evaluation, objective formulation, optimization, and post-processing is accessible to other researchers without restriction.

Functionally, DeVana is designed to connect high-level vibration performance requirements to physically realizable absorber configurations. It can model coupled primary-structure–plus-absorber systems with up to five total degrees of freedom, where two degrees of freedom are attributed to the main system and up to three additional degrees of freedom are reserved for the absorber. Within that range, DeVana assembles the coupled equations of motion, computes the dynamic response of the combined system, and evaluates the FRF. This is essential in the present work, because all design targets are expressed directly in the frequency domain (resonant peak locations, amplitudes, bandwidth shaping, etc.), and the optimization is driven by how well the FRF of the tuned system matches those targets.

The workflow in DeVana is organized around constrained optimization. The user selects which absorber parameters will be tuned, and each of those parameters is normalized and restricted to lie in $[0, 1]$. The user then defines performance objectives for the coupled system, such as the desired frequencies and amplitudes of the dominant peaks and the allowable bandwidth of elevated response, and assigns weights to these objectives to indicate their relative importance. The user also specifies optimization settings such as population size, number of generations, and stopping tolerance. Once this problem is defined, DeVana automatically generates candidate absorber designs, evaluates their performance, and iteratively improves them.

Although DeVana supports multiple metaheuristic solvers, including Particle Swarm Optimization and Differential Evolution, and etc. the present paper focuses on the Genetic Algorithm (GA) engine, which is used as the main optimizer in this study.

In DeVana, the Genetic Algorithm can be run either with fixed (static) genetic settings or with adaptive control. When adaptive control is enabled, the software can apply several adaptive schemes in which crossover and mutation rates are automatically adjusted during the run. For example, mutation can be increased when the population starts to collapse around a narrow region of the design space, which helps avoid premature convergence to a poor local minimum, while crossover can be intensified when several strong solutions appear in the same region, so that the algorithm focuses on exploiting and refining that region. This adaptive exploration–exploitation balance is particularly important for DVA design problems, which are highly multimodal: many different parameter combinations can produce locally acceptable vibration behavior, but only a limited subset satisfy all frequency-response constraints simultaneously while remaining sparse and practically realizable.

All main GA controls, population size, maximum number of generations, tolerance for convergence, etc. are exposed to the user. During optimization, DeVana records generation-by-generation data such as best fitness, median fitness, and indicators of population diversity. This information is used internally to steer the adaptive GA behavior and is also made available for analysis after the run.

A key feature of DeVana, and one that is critical for engineering use, is that it treats optimization results as data to be interpreted, not just as a final number. After a run, DeVana provides structured post-processing tools that:

- plot convergence histories to show how (and how quickly) the fitness decreased,
- track how each absorber parameter evolved across generations (for example, which parameters are consistently driven toward zero by the sparsity penalty and which remain active),
- compare the final FRF of the optimized design against the user-specified FRF targets, and
- summarize results statistically across multiple runs to evaluate robustness and repeatability.

This is particularly important given the role of sparsity in the proposed formulation. The optimization problem in this work is not only "match the desired FRF," but also "do so with the fewest effectively active absorber parameters." DeVana makes that trade-off explicit and inspectable: by examining repeated runs, the user can identify a minimal set of absorber parameters that reliably remain active, which points directly to absorber designs that are both high-performing and practically manufacturable.

Genetic Algorithm implementation

Figure 1 illustrates the workflow of the GA optimization process implemented in DeVana for tuning DVA parameters. The process begins with the definition of parameter constraints, followed by the generation of an initial random population of candidate DVA configurations. Each candidate solution is evaluated using a predefined fitness function, and the population is then ranked through non-dominated sorting. Fitness-based sorting is performed to assign ranks (e.g., first, second, etc.), and crowding distance is computed to maintain diversity within the population. A two-at-a-time comparison strategy identifies the most promising individuals, upon which adaptive crossover and mutation operations are performed to generate new candidate solutions. An elitism mechanism preserves the best individuals by combining the previous fronts with the newly created population before replacing the old population. The updated population is then subjected to a new generation of

evaluation. This iterative process continues until the optimal set of DVA parameters satisfies a predefined convergence tolerance, at which point the algorithm terminates. The flowchart highlights DeVana's structured and robust implementation of GA, ensuring both solution quality and computational efficiency.

This GA process is intended to obtain high-quality local optima rather than to guarantee a single global optimum. The design space for DVA tuning is highly multimodal, and multiple distinct absorber configurations can achieve acceptable vibration performance. DeVana's role, therefore, is not only to produce one numerically minimal point, but to identify practically meaningful solutions that satisfy dynamic targets while remaining simple enough to manufacture. In extended studies building on this framework, repeated runs of this process are used to collect multiple such locally optimal solutions and infer stable parameter ranges for each design variable, rather than reporting only one "best" point. This range-based interpretation is more valuable for engineering design, because it provides the designer with feasible intervals of implementation rather than a single brittle setting. Figure 1 summarizes this overall philosophy: structured GA search, adaptive genetic control, sparsity-aware fitness evaluation, elitist selection, and convergence to realizable absorber designs within defined tolerances.

In DeVana, optimization is guided by a composite fitness function that balances performance matching, numerical robustness, and physical simplicity of the absorber. The fitness used by the genetic algorithm is defined as:

$$Fitness = |C_s - 1| + PE + SP \quad (9)$$

and each of the three terms is described below:

- **Singular-criterion deviation $|C_s - 1|$:** The term C_s is a scalar "singular criterion" that encodes the overall design quality. It is constructed from a set of design metrics $\{C_i(\theta)\}$, each of which measures one physical target of interest
- **Percentage Error (PE):** The second term, PE (percentage error), enforces that each individual target is actually met, not just balanced in the weighted sum C_s. While $|C_s - 1|$measures global agreement, different metrics could, in principle, compensate for each other numerically: one could overshoot while another undershoots, giving a deceptively good C_s. To prevent this, PE is computed as the accumulated relative error across all specified targets:

$$PE = \sum_i \left| \frac{C_i(\theta) - T_i}{T_i} \right| \quad (10)$$

- **Sparsity penalty (SP):** The third term, SP, is a sparsity-inducing penalty that promotes DVA designs that are as simple as possible. The sparsity penalty is defined as:

$$SP = \alpha \sum_{j=1}^{n_s} \theta_j \quad (11)$$

where $\alpha > 0$ is a user-selected sparsity weight. This is effectively an ℓ_1-type regularization: it increases linearly with the number and magnitude of "active" absorber parameters.

Through normalization, all terms are rendered dimensionless and comparable, such that distortion of scale is avoided when objectives with differing physical units are added. By

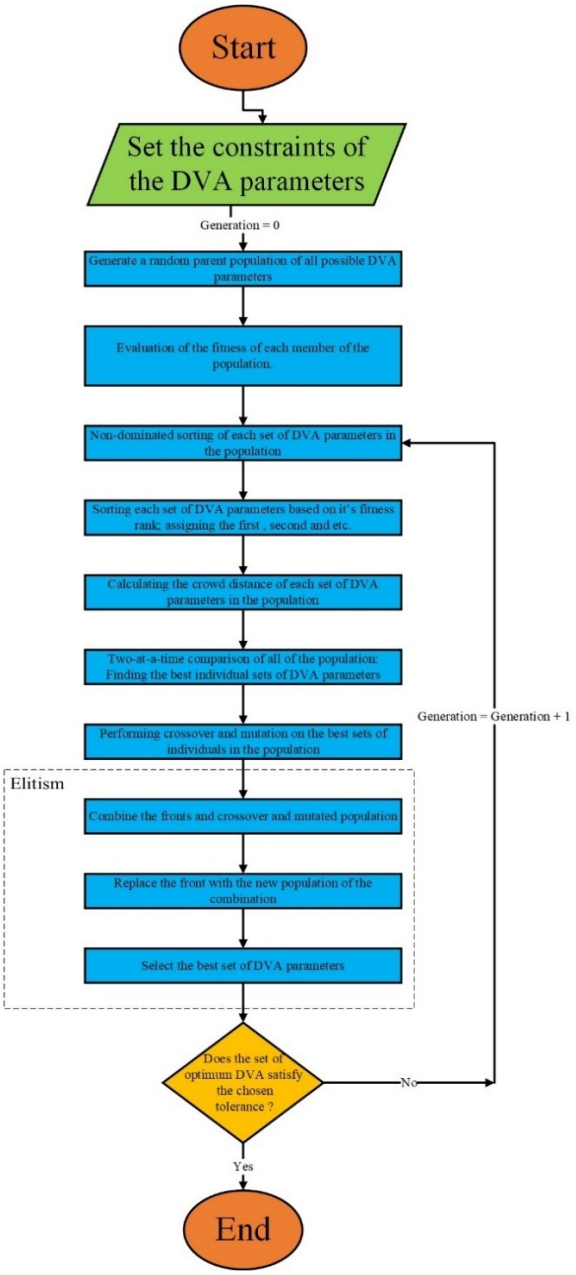

Figure 1. Flowchart of the Genetic Algorithm (GA) optimization process implemented in DeVana for tuning Dynamic Vibration Absorber (DVA) parameters.

constraining the nonnegative weights to sum to one, the score's range and interpretation are preserved as additional objectives are appended; a value of one is retained as an indicator that all targets are met. Scalability from simple to richly specified problems is thereby achieved, and priorities are tuned through the weights without alteration of the optimization framework.

Benchmarking the Singular Criterion in a Fully Coupled 1-DOF–1DOF System

1DOF–1DOF fully coupled system

To evaluate the accuracy and reliability of the singular criterion-based optimization approach, a benchmark is performed using a fully coupled 1DOF–1DOF mechanical system, consisting of a single-degree-of-freedom (1DOF) primary mass and a single-degree-of-freedom (1DOF) dynamic vibration absorber (shown in Fig.2). In this configuration, both the primary system and the DVA are coupled not only to each other but also to two moving bases, an upper base and a lower base, through individual sets of spring, damper, and inerter elements. The primary mass is connected to the upper and lower bases via springs and dampers. The DVA is then attached to the main mass through a dedicated spring-damper-inerter system, forming the absorber path, and is also independently coupled to both bases through spring-damper-inerter elements. An external force is applied to the primary mass to simulate real excitation conditions. This **fully coupled 1DOF–1DOF system** represents a highly interconnected model where all nodes are dynamic, no base is fixed, and every component participates in energy exchange. It represents the most comprehensive and general configuration of a vibration absorber within a 2DOF framework, ensuring that the validation process is free from physical simplifications or idealized assumptions. The system structure follows the internal indexing conventions used in the ***"DeVana"*** software (version 0.4.1), which supports up to five degrees of freedom. Although the physical system used here is simplified to two active degrees of freedom for demonstration purposes, the variable names and reference points remain consistent with those used in DeVana. The full 5DOF system model and indexing details can be found in the program's documentation[27]. This benchmark setup provides a minimal yet fully expressive framework for validating the performance of the singular criterion under complex, realistic coupling conditions.

Equations of motion of the fully coupled system

Let q be the system's generalized coordinate. $U(t)$ and $u(t)$, respectively, represent the main system and DVA displacements at time t.

$$q = \begin{bmatrix} U(t) \\ u(t) \end{bmatrix}, \dot{q} = \begin{bmatrix} \dot{U}(t) \\ \dot{u}(t) \end{bmatrix}, \ddot{q} = \begin{bmatrix} \ddot{U}(t) \\ \ddot{u}(t) \end{bmatrix} \tag{12}$$

The equation of motion can be expressed using the dimensional parameters as:

$$[M][\ddot{q}] + 2\zeta_{dc}\omega_{dc}[C][\dot{q}] + \omega_{dc}^2[K][q] = [F] \tag{13}$$

where:

$$[M] = \begin{bmatrix} 1+\beta_1 & -\beta_1 \\ -\beta_1 & \mu+\beta_1+\beta_7+\beta_8 \end{bmatrix} \tag{14}$$

$$[C] = \begin{bmatrix} 1+N+\nu_1 & -\nu_1 \\ -\nu_1 & \nu_1+\nu_7+\nu_8 \end{bmatrix} \tag{15}$$

$$[K] = \begin{bmatrix} 1+\Lambda+\lambda_1 & -\lambda_1 \\ -\lambda_1 & \lambda_1+\lambda_7+\lambda_8 \end{bmatrix} \tag{16}$$

$$[F] = \begin{bmatrix} F_1 \\ F_2 \end{bmatrix} \tag{17}$$

$$F_1 = F' + 2\zeta_{dc}\omega_{dc}\left(\dot{U_{Low}} + N\dot{U_{Up}}\right) + \omega_{dc}^2\left(U_{Low(t)} + \Lambda U_{Up(t)}\right) \tag{18}$$

$$F_2 = \beta_7\ddot{U_{Low}} + \beta_8\ddot{U_{Up}} + 2\zeta_{dc}\omega_{dc}\left(\nu_7\dot{U_{Low}} + \nu_8\dot{U_{Up}}\right) + \omega_{dc}^2\left(\lambda_7 U_{Low(t)} + \lambda_8 U_{Up(t)}\right) \tag{19}$$

To enable normalized analysis and optimization, the system's dimensional parameters are carefully specified. The ratio of mass, represented by μ, is defined as ($\mu \equiv \frac{m}{M}$), representing the ratio of the DVA mass (m) to the main mass M. The inerter ratios, β_1, β_7, and β_8, are defined for each respective inerter coefficient as ($\beta_i \equiv \frac{b_i}{M}$), where b_i are the inerter coefficients. Stiffness ratios are represented by λ_1, λ_7, λ_8, and Λ, defined by ($\lambda_i \equiv \frac{k_i}{K_1}$) for ($i = 1, 7, 8$), and ($\Lambda \equiv \frac{K_2}{K_1}$), where k_i are the stiffness coefficients and K_1 and K_2 are the system stiffnesses. Similarly, damping ratios ν_1, ν_7, ν_8, and N are defined as ($\nu_i \equiv \frac{c_i}{C_1}$) and ($N \equiv \frac{C_2}{C_1}$), where c_i are the damping coefficients and C_1 and C_2 are the system damping coefficients. The decoupled natural frequency ω_{dc} and the damping ratio ζ_{dc} are defined using the lower base parameters as ($\omega_{dc} \equiv \sqrt{\frac{K_1}{M}}$) and ($\zeta_{dc} \equiv \frac{C_1}{2M\omega_{dc}}$), respectively. Additionally, the parameter $F'_{(t)}$ is defined as $F'_{(t)} \equiv \frac{F_{(t)}}{M}$, normalizing the external force by the main system mass.

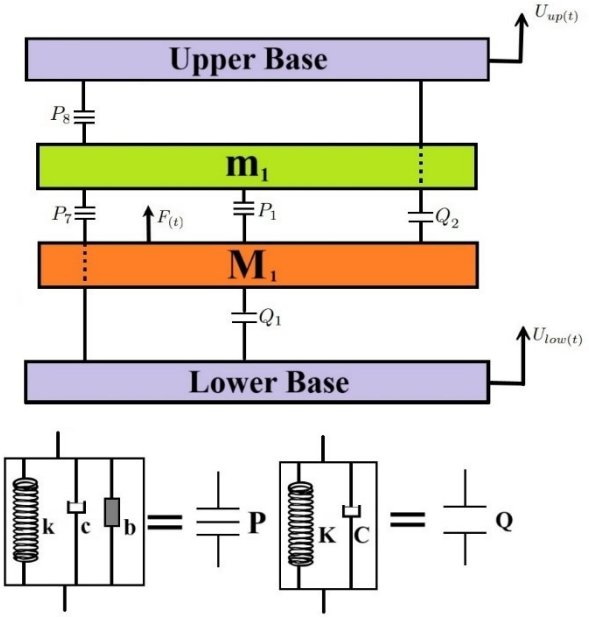

Figure 2. Schematic of the fully coupled 1DOF–1DOF benchmark system used for validation of the singular criterion.

The semi-analytical method involves proposing a solution for the generalized coordinate of the system, which has unknown

coefficients but a known structure. The unknown coefficients are then determined by applying boundary and initial conditions. The analysis assumes that the bases and the harmonic excitation are in harmonic synchrony, meaning they all function at the same frequency of ω at the same time. Thus, the generalized coordinate system can be written as the steady-state response as:

$$q = \begin{bmatrix} U(t) \\ u(t) \end{bmatrix} = \begin{bmatrix} A \\ a \end{bmatrix} e^{j\omega t} \tag{20}$$

Where ω is the excitation frequency and A and a are the vibration amplitudes of the main and DVA systems, respectively. Harmonic excitation of the main system's mass and the harmonic motion of the bases can be further characterized as:

$$F'_{(t)} = f e^{j\omega t} \tag{21}$$

$$U_{Low(t)} = A_{Low} e^{j\omega t} \tag{22}$$

$$U_{Up(t)} = A_{Up} e^{j\omega t} \tag{23}$$

The amplitude of the main system's excitation is denoted by f, while A_{Low} and A_{Up} represent the amplitudes of the motion of the lower and upper bases, respectively. By replacing into the, the equation of motion of the system may be reformulated as:

$$\begin{bmatrix} A \\ a \end{bmatrix} = \omega_{dc}^2 \left((-\Omega^2 [M] + 2j\omega\zeta_{dc}\Omega [C] + [K]) e^{j\omega t} \right)^{-1} [f] \tag{24}$$

The steady-state harmonic response is presumed because the primary analysis targets the frequency response functions (FRFs), which characterize the system's behavior under harmonic forcing. This approach involves solving the equations in the frequency domain, where the response is expressed as a steady oscillation at each excitation frequency. This method is valid under the following conditions:

- The excitation is purely harmonic and sinusoidal.
- The damping present in the system is linear and proportional (e.g., viscous damping).
- Initial transient effects have decayed, meaning the system response has stabilized into a steady oscillation.

However, this assumption is not suitable for transient or non-harmonic systems, such as those subjected to random, impulse, or non-periodic excitations. In such cases:

- The equations of motion need to be developed in the time domain as second-order differential equations with time-dependent force inputs.
- Numerical integration techniques such as the Newmark-beta or Runge-Kutta methods are used to simulate the transient response.
- For random excitations, spectral or statistical methods are employed to analyze the response, focusing on probability densities and power spectral densities rather than steady-state oscillations.

Finally, the steady-state harmonic response assumption is proper only under harmonic excitation conditions. For transient or irregular excitations, the equations of motion must be formulated in the time domain, and dynamic simulation or spectral analysis techniques should be employed.

System Parameters

In order to evaluate the effectiveness of the introduced GA algorithm on the singular criterion, a numerical analysis was carried out using arbitrary values for the main system, listed in Tab.1.

Table 1: The main system parameters value

Main System Parameters	Value
$\boldsymbol{\Lambda}$	1
$\boldsymbol{N}$	1
$\boldsymbol{A_{Up} = A_{Low}}$	0.0001
$\boldsymbol{F}$	100
$\boldsymbol{\omega_{dc}}$	1000
$\boldsymbol{\zeta_{dc}}$	0.01

All DVA design variables used in the optimization are normalized and constrained to lie within the interval [0, 1]. The target values and associated weights for this specific benchmark example are as follows: The target bandwidth is set to 1000 rad/s, carrying a weight of 0.3; the primary system peak positions are set at 1000 rad/s and 2000 rad/s, with individual weights of 0.35 each. These weighting coefficients reflect the design priorities in this benchmark case. The dominant peaks of the primary system govern the most critical aspects of vibration suppression (i.e., where the main resonances occur and how they are shaped), so each peak-related objective is assigned a higher weight (0.35) to ensure that the optimizer strongly penalizes any deviation in their frequency placement and amplitude. The bandwidth objective, while still important for controlling the overall spread of energy in the response, is treated as secondary and is therefore assigned a slightly lower weight (0.3). All weights are normalized so that they sum to 1, which keeps the combined performance metric $C_s$dimensionless and directly interpretable: values of $C_s$close to 1 correspond to a response that satisfies the prioritized design targets according to the specified trade-off between precise peak control and acceptable bandwidth. Together, these values direct the optimization process toward balanced performance in terms of frequency response and amplitude reduction. The sparsity penalty weight is set at 0.0002, meaning the fitness score increases in proportion to the total sum of DVA values. The target tolerance is fixed at 0.0012, which ensures that, even in the best-case scenario, the solution converges with only a limited number of DVA parameters active, although this might not happen due to the convergence issues or the fact that the solution is unavailable but it points out how can we have the best vector of the DVA solution with the least amount of the DVA parameters. This method amplifies the

practicality of the fitness function that we have defined that is very close line and trade off of different targets for the design of the DVA.

Genetic algorithm setup

The optimization targets are selected to reward performance while discouraging overuse of DVA components. The target bandwidth is 1000 rad/s with a weight of 0.30, and the primary system peak positions are set at 1000 rad/s and 2000 rad/s with weights of 0.35 each. To promote compact designs, the fitness includes a sparsity term is added per active DVA parameter. This setup steers the search toward the best achievable frequency response with the fewest parameters, limits unnecessary components, and improves implement ability. In cases where feasibility or convergence prevents exact attainment of the targets, the framework still favors the sparsest high-performing solution.

Validation of the Method

To show that this strategy is consistent with established tuned absorber theory, we compare it to the classical H_∞ approach of Asami et al.[28] In that approach, the absorber is tuned so that the two dominant resonance peaks in the primary mass frequency response are equal in amplitude and as low as possible. This equal peak rule is widely taken as the practical form of H_∞ optimality for passive dynamic vibration absorbers. Asami's analytical H_∞ solutions, assume a simpler two degree of freedom model. In that classical model, there is one primary mass attached to ground and one absorber mass attached to the primary mass through a single spring and a single damper. There are no inerters and no second base. In this reduced model, the absorber is defined only by two tuning parameters λ_1 and ν_1. The goal is to split the original main resonance into two peaks that sit near the same amplitude, about 2000 in nondimensional FRF magnitude units, and to make the difference between those two peak amplitudes as small as possible. The structural properties imposed in this benchmark are $\omega_{dc} = 14.14$ rad/s, $\zeta_{dc} = 0.24$, and $\mu = 0$. Three tuning strategies are applied to this same simple two degree of freedom model. The first strategy is the Asami first order solution, which is the closed form H_∞ tuning for a first order absorber and gives one optimal pair (λ_1, ν_1). The second strategy is the Asami second order solution, which is an analytical extension that includes higher order absorber dynamics. The third strategy is the genetic algorithm with the singular criterion. For this validation study, the genetic algorithm is restricted to the same two parameters λ_1 and ν_1, and access to any additional coupling paths from the fully coupled benchmark is intentionally removed. The objective for all three methods is identical. Each method attempts to minimize the absolute difference between the first and second resonance peak amplitudes of the primary mass.

Table 2 lists the optimal absorber parameters and the resulting peak mismatch. Lower difference corresponds to better equalization of the two main peaks.

Table.2: The validation of the three different methods using H_∞ method

Method	(λ_1)	(ν_1)	Difference between the first and second peak amplitudes
Asami first order	0.1525	4.568	1220.33
Asami second order	0.1250	4.041	1980.57
Genetic Algorithm	0.3101	0.2239	574.00

The genetic algorithm result gives the smallest peak mismatch, with a mismatch of 574. The first order Asami result produces a mismatch of 1220.33, and the second order Asami result produces a mismatch of 1980.57. The mismatch produced by the genetic algorithm is therefore less than half of the first order value and more than three times lower than the second order value. The genetic algorithm also converges to a different damping region. The Asami solutions call for effective damping ν_1 on the order of 4 to 5, while the genetic algorithm result uses $\nu_1 = 0.2239$. At the same time, the stiffness ratio λ_1 increases from about 0.125 to 0.3101. This behavior shows that strong peak equalization does not require extremely high damping if the parameters are identified by direct FRF shaping.

Results and Discussion

Frequency Response and Optimum DVA parameters

The FRFs of the primary mass with and without the optimized DVA are shown in Fig.3. The frequency range extends from 0 to 2200 Hz. In the absence of the DVA, a single resonance peak is observed within 1000 to 2000 Hz, which is not ideal for the specified avoidance band. With the DVA included, two peaks are observed near 1000 Hz and 2000 Hz, and the interior of the band remains without a resonance peak. Outside 1000 to 2000 Hz, the response levels of the two cases are similar and remain small.

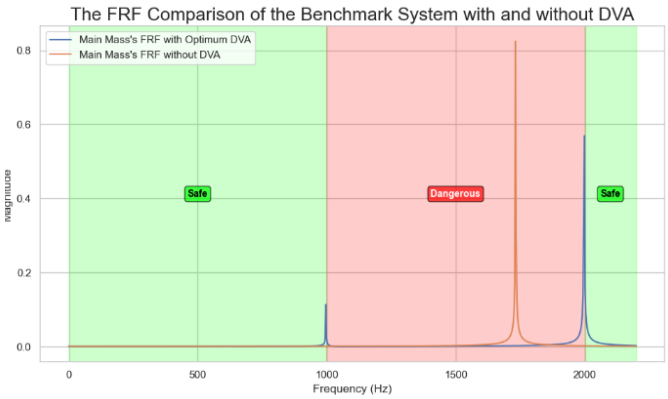

Fig.3: Frequency response of the primary system without DVA and with the optimized DVA.

An avoidance band of 1000 to 2000 Hz had been specified for resonant behavior. With the optimum DVA, resonances within this band were prevented, and the dominant peaks were placed at the band edges. The targeted bandwidth was therefore protected, and the design requirement was satisfied with minimal in-band amplification.

The optimum DVA parameter set was obtained as $\beta_1 = 0.0152, \beta_7 = 0.5509, \beta_8 = 0, \lambda_1 = 0.8235, \lambda_7 = 0.2580, \lambda_8 = 0.0789, \mu_1 = 0.3671$, with $\nu_1 = 0, \nu_7 = 0$, and $\nu_8 = 0$. The zero ν values indicate that these couplings were not required, so a sparse and efficient configuration was achieved with only the necessary terms active.

The total fitness equals 0.001206, composed of 40.8% from the primary objective term, 34.7% from the sparsity penalty, and 24.5% from the percentage-error term as shown in Fig.5.

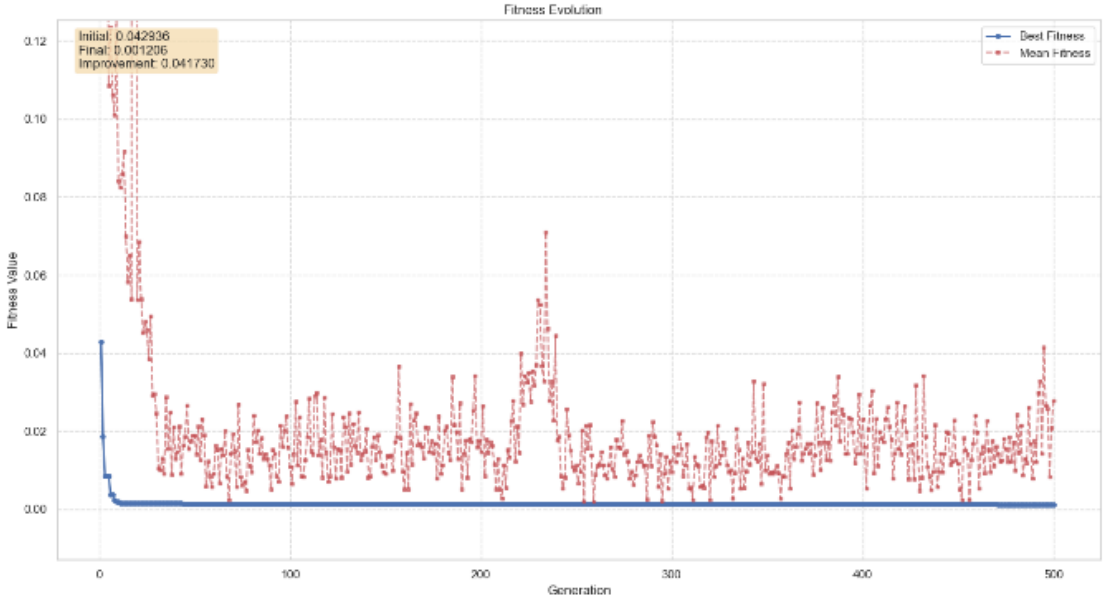

Fig.4: Fitness evolution over 500 generations.

In Fig.4, best and mean fitness values over 500 generations are reported. The initial best fitness equals 0.042936 and the final best fitness equals 0.001206, which corresponds to an absolute improvement of 0.041730. The mean fitness shows a rapid early decrease, followed by fluctuations around the 0.01 to 0.02 range with occasional spikes, while the best fitness remains near the lower envelope after the first few tens of generations. A sharp early reduction is indicated, consistent with efficient coarse exploration by the GA. The persistent gap between mean and best fitness suggests that population diversity was maintained. The continuous gap observed between the best fitness and the average fitness in Figure 4 primarily indicates preservation of population diversity rather than a problem of premature convergence or getting stuck in local optima. Maintaining such a gap is generally desirable in evolutionary algorithms as it ensures that the population retains a variety of candidate solutions, allowing continued exploration of the solution space and reducing the risk of convergence to suboptimal local minima.

If this gap were absent or very small, it could imply that the population has lost diversity and the algorithm might be trapped in local optima. However, in our case, the sustained difference between the best and average fitness values corroborates that the population has effectively balanced exploration and exploitation during the optimization process, thereby preventing premature convergence.

Thus, the gap in Figure 4 reflects the genetic algorithm's healthy performance in preserving diversity and optimizing towards the global optimum rather than indicating any issue with local optima entrapment.

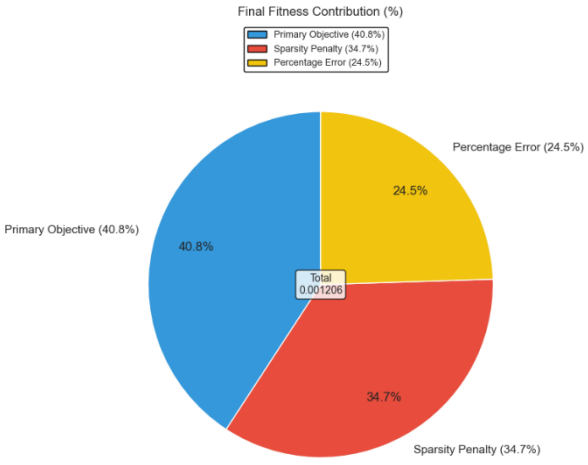

Fig.5: Final fitness decomposition in the best solution.

A substantial contribution from the sparsity penalty is evidenced during optimization, yet the final value remains small, which indicates that the primary objective was achieved without reliance on many tuning variables. The near-zero values assigned to most parameters demonstrate that only a minimal subset was required to meet the targets, consistent with a parsimonious DVA configuration that avoids unnecessary elements.

In Fig.6, the per-generation improvement rate is plotted for all 500 generations. Large spikes are confined to the initial phase, after which the rate approaches zero with only sporadic small increases. The average improvement rate is annotated as 8.4×10^{-5} per generation. Rapid improvements are concentrated in the early generations, followed by diminishing changes, which is characteristic of convergence to a stable optimum. The near-zero rates observed through the latter part of the run indicate that only minor local refinements were occurring, and that the solution had effectively stabilized.

In Fig.7, μ_1 is tracked across 500 generations. It was initialized at 0.393887 and was recorded at 0.367131 in the final generation, a net decrease of 0.026756. A linear trend was fitted with slope -3.41×10^{-4} per generation. The average generation to generation increment was -5.4×10^{-5}.
The observed span was 0.2159, and the standard deviation was 0.0535. A gradual downward drift with small step sizes is indicated, followed by stabilization in later generations. Convergence was dominated by a steady downward drift with diminishing step sizes. Variability was reduced after the early generations, and no sustained oscillations were observed. The final value lies well inside the feasible range, which indicates that μ_1 remains an active parameter.
Parameter-wise convergence is summarized in Figures 8 through 10, with the β parameters in Figure 8, the λ parameters in Figure 9, and the ν parameters in Figure 10. For each parameter, the trajectory across generations is shown together with its value distribution and summary metrics.
In Fig. 8 (a), β_1 is tracked for 500 generations. The parameter was initialized at 0.029003 and was recorded at 0.015239 in the final generation, a net decrease of 0.013764. A fitted linear trend shows a slope of -6.0×10^{-6} per generation. The average generation to generation increment was -2.8×10^{-5}. The observed range was 0.0307, with a standard deviation of 0.0028. The value distribution is narrow and centered near 0.019.

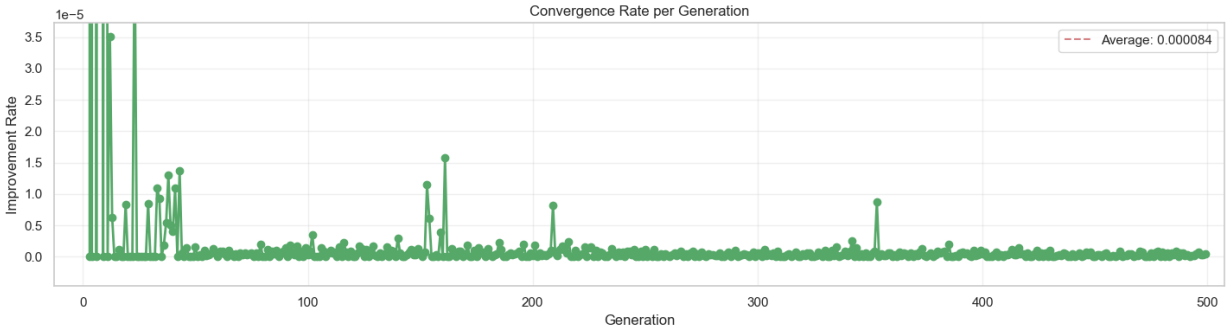

Fig.6: The per-generation improvement rate over 500 generations.

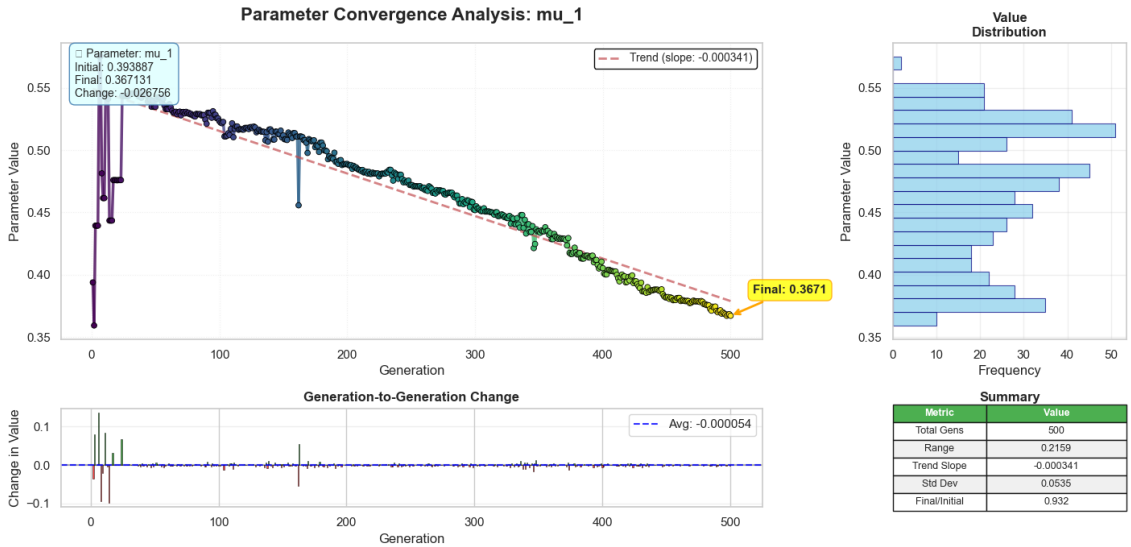

Fig.7: Convergence of μ_1 across 500 generations

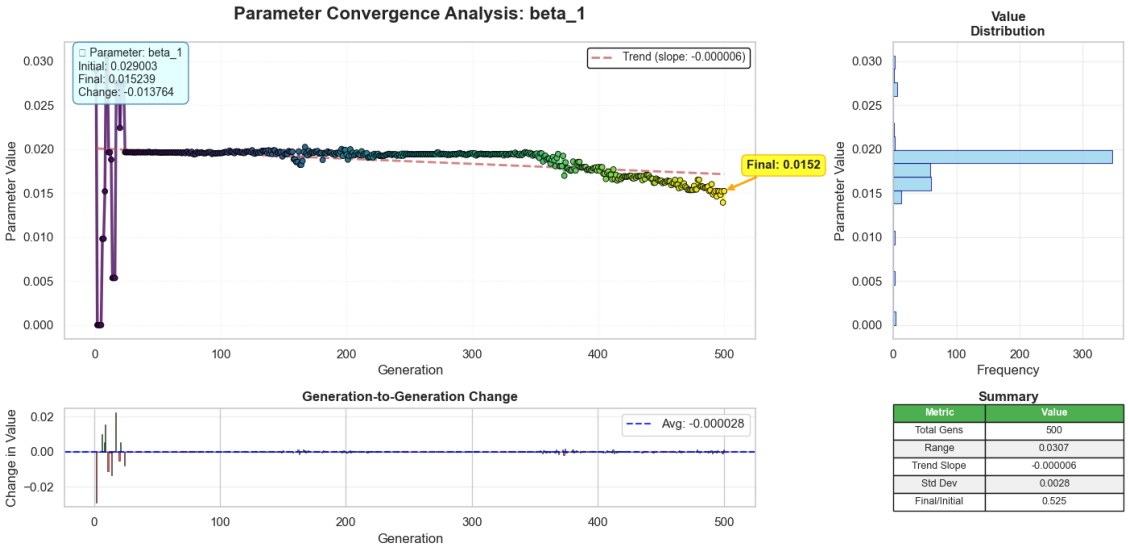

(a)

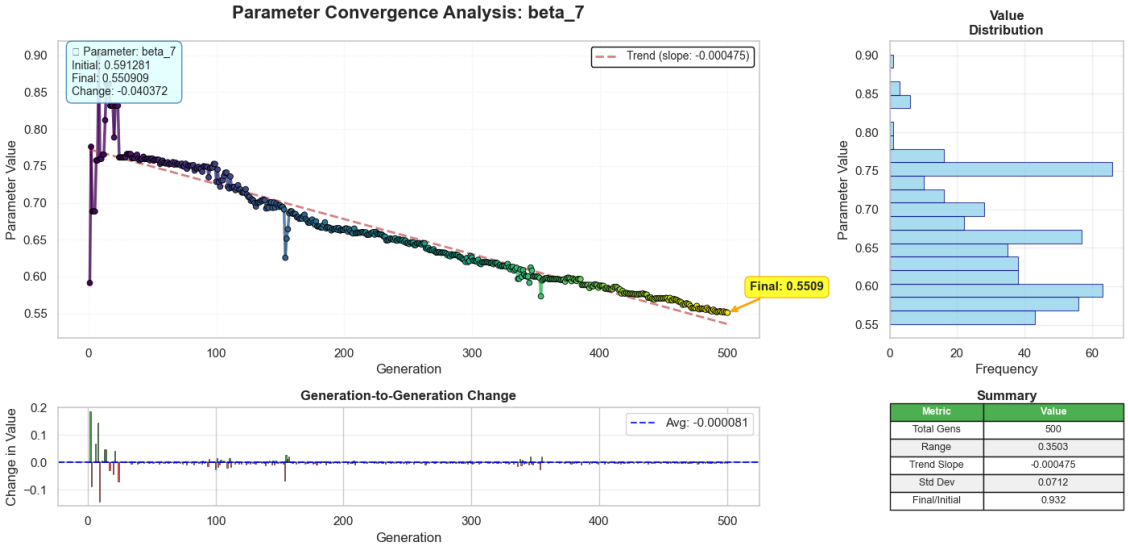

(b)

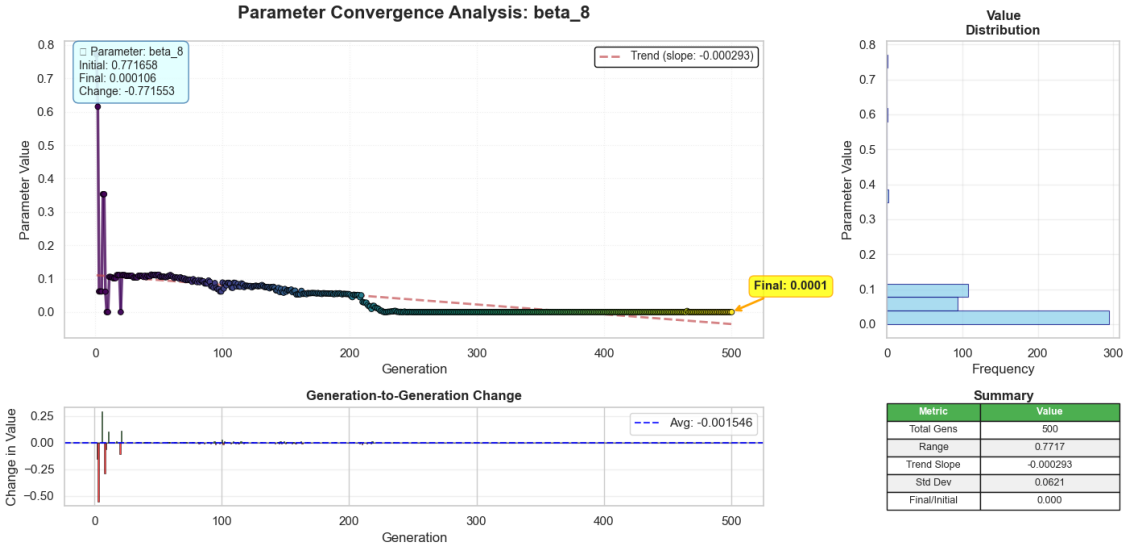

(c)

Fig.8: Convergence of β parameters: (a) β_1, (b) β_7, (c) β_8.

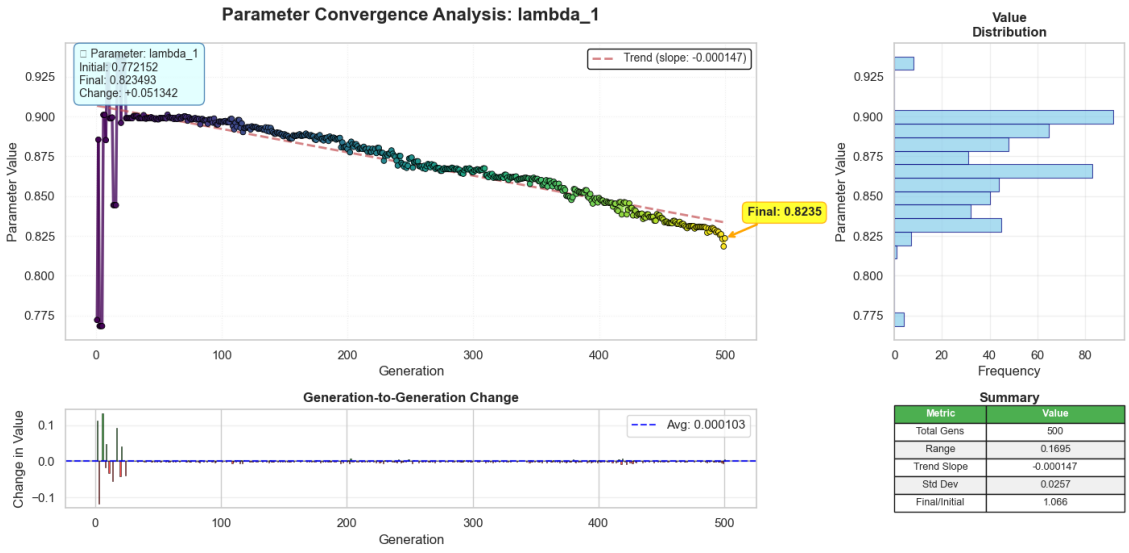

(a)

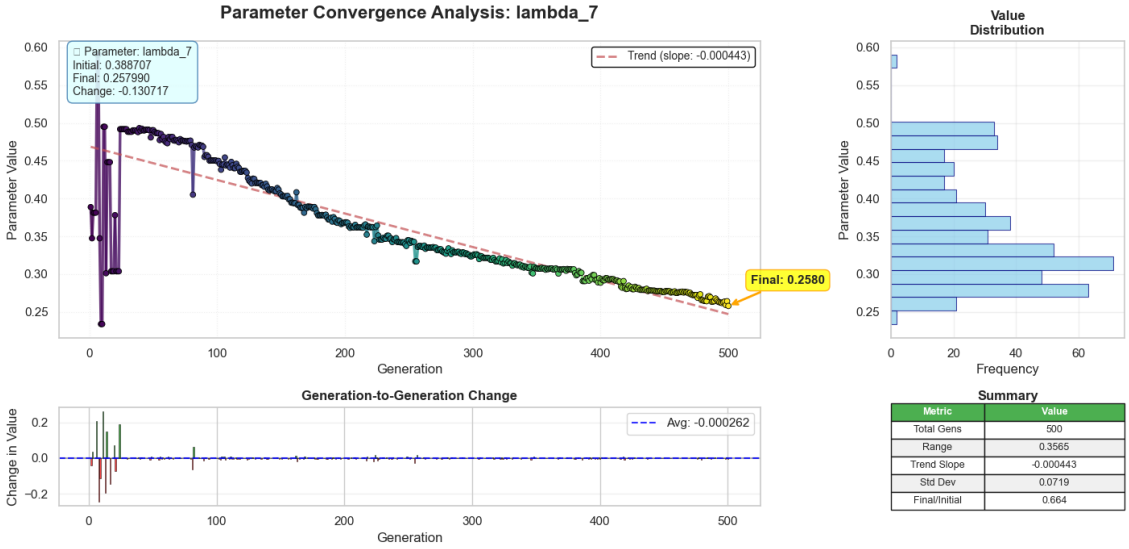

(b)

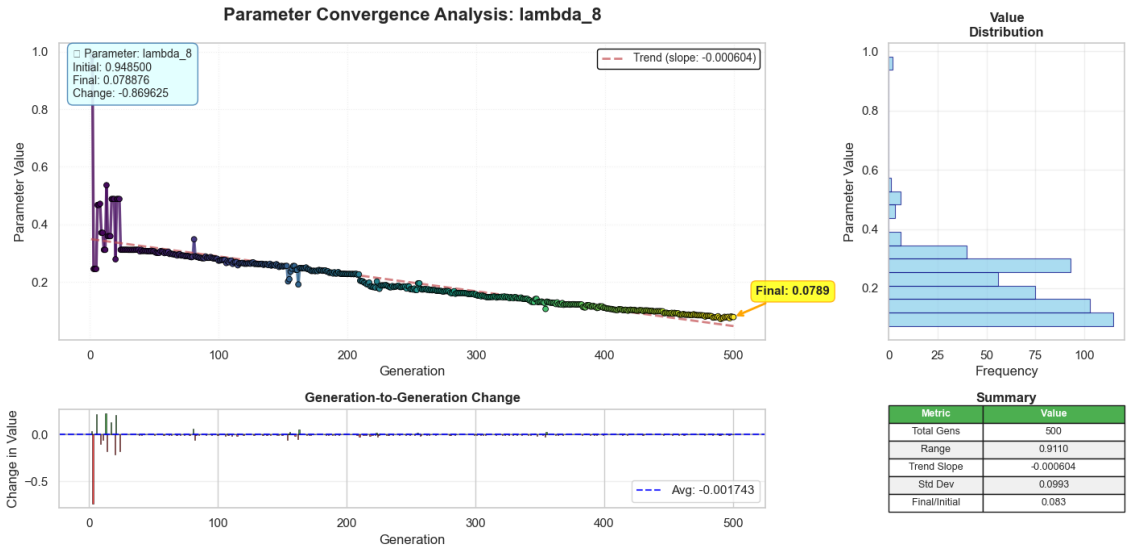

(c)

Fig.9: Convergence of λ parameters: (a) λ_1, (b) λ_7, (c) λ_8.

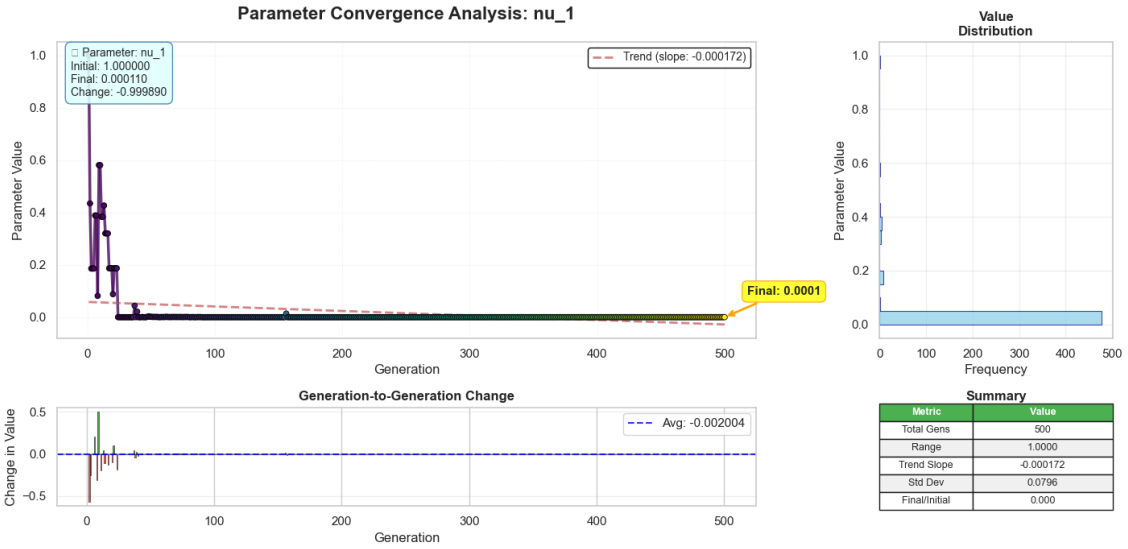

(a)

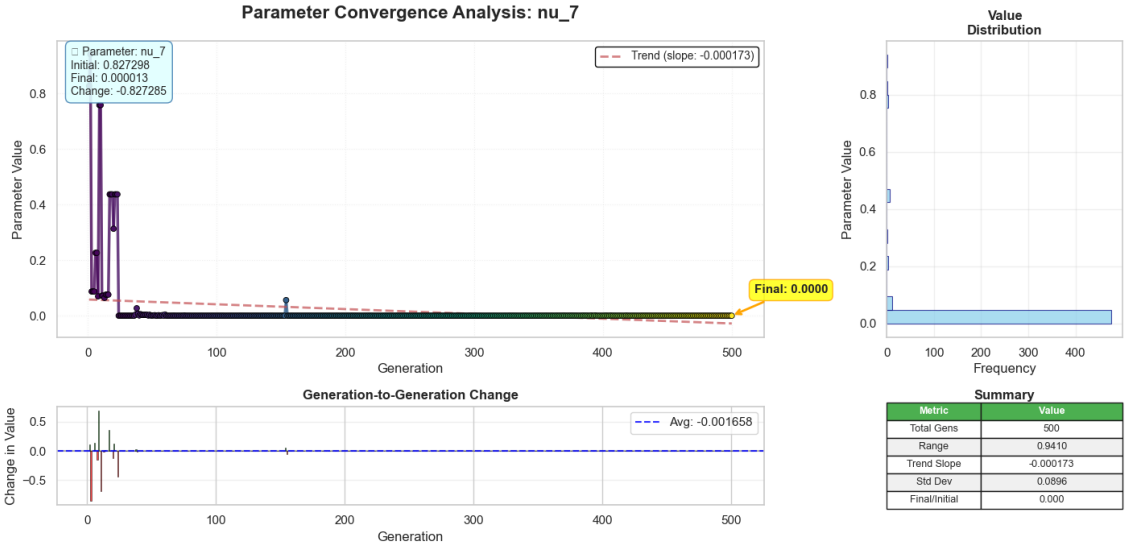

(b)

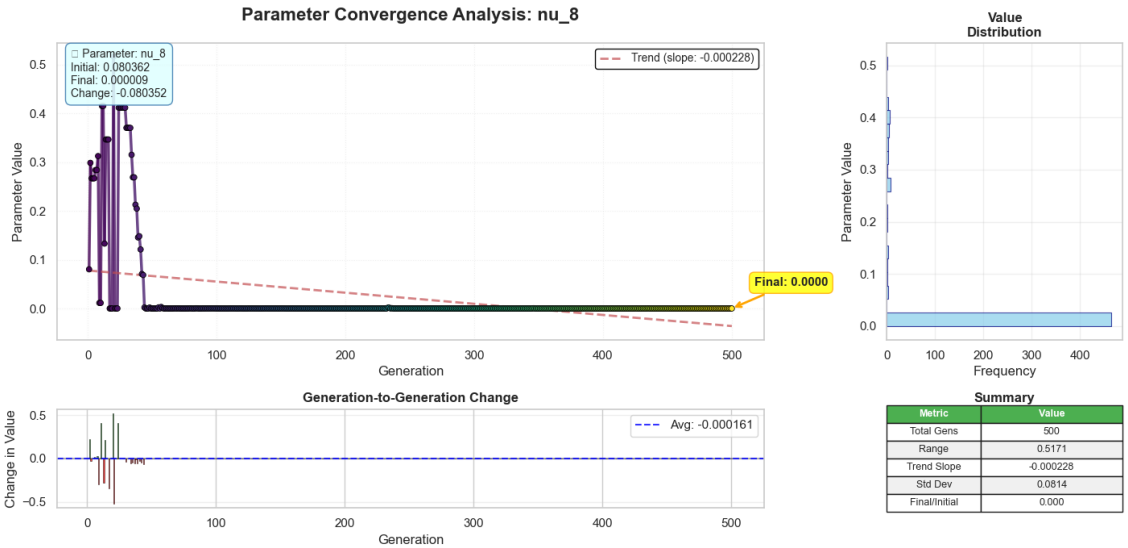

(c)

Fig.10: Convergence of ν parameters: (a) ν_1, (b) ν_7, (c) ν_8.

A near-constant trajectory followed by a mild late-stage decline is indicated. Stabilization occurred well inside the feasible region. β_1 was therefore retained as a small but active tuning variable at the optimum, consistent with fine adjustments rather than boundary-driven behavior. In Fig. 8 (b), β_7 is tracked for 500 generations. The parameter moved from 0.591281 to 0.550909, a net change of −0.040372. The fitted trend has slope -4.75×10^{-4} per generation. The average increment per generation was -8.1×10^{-5}. The range measured 0.3503 and the standard deviation was 0.0712. A steady downward drift with diminishing step sizes is observed, followed by sustained stabilization. The relatively large magnitude of β_7 compared with β_1 suggests that β_7 played a primary role in shaping the response of the FRF. In Fig. 8 (c), β_8 is monitored across 500 generations. The parameter changed from 0.771658 to 0.000106, a reduction of 0.771553. The fitted trend shows slope -2.93×10^{-4} per generation. The average increment per generation was −0.001546. The observed range was 0.7717 and the standard deviation was 0.0621. The histogram indicates heavy mass near zero after the early generations. A rapid early collapse toward zero is indicated, after which only negligible adjustments occurred. The near-zero final value implies that β_8 was effectively pruned by the optimization, which is consistent with the sparsity objective and with avoidance of unnecessary tuning parameters.

In Fig. 9 (a), λ_1 is tracked over 500 generations. The parameter was initialized at 0.772152 and was reported at 0.823493 in the final generation, a net increase of 0.051342. A linear trend with slope -1.47×10^{-4} per generation was fitted, while the average generation to generation increment measured 1.03×10^{-4}. The observed range was 0.1695 with a standard deviation of 0.0257. The value distribution is concentrated between 0.84 and 0.90. A brief early adjustment was followed by a long, slowly varying trajectory that settled inside the feasible region. The interior final value indicates that λ_1 remained an active tuning variable. In Fig. 9 (b), λ_7 is shown for 500 generations. The parameter moved from 0.388707 to 0.257990, a reduction of 0.130717. The fitted trend exhibited slope -4.43×10^{-4} per generation. The average increment per generation was -2.62×10^{-4}. The span across the run was 0.3565 and the standard deviation was 0.0719. A steady downward drift with diminishing steps was observed. The final value suggests that λ_7 contributed to the performance of the DVA. In Fig. 9 (c), λ_8 is monitored across 500 generations. The parameter decreased from 0.948500 to 0.078876, a net change of −0.869625. The fitted trend had slope -6.04×10^{-4} per generation, and the average generation to generation increment was -1.743×10^{-3}. The observed range was 0.9110 with a standard deviation of 0.0993. The distribution shows heavy mass near small values in later generations. A rapid decay toward the lower end of the explored range is indicated, after which only minor refinements occurred. The small final value implies that λ_8 was effectively down-weighted by the optimization, consistent with the sparsity objective and with avoidance of unnecessary tuning influence.

Across Figures 10 (a), 10 (b), and 10c, the convergence of ν_1, ν_7, and ν_8 over 500 generations is documented. Initial values of 1.000000, 0.827298, and 0.080362 were recorded for ν_1, ν_7, and ν_8, and final values of 0.000110, 0.000013, and 0.000009 were obtained, respectively. Net decreases of 0.999890, 0.827285, and 0.080353 were produced. The observed ranges were 1.0000 for ν_1, 0.9410 for ν_7, and 0.5171 for ν_8, with standard deviations of 0.0796, 0.0896, and 0.0814. Linear trend lines were fitted with slopes of -1.72×10^{-4}, -1.73×10^{-4}, and -2.28×10^{-4} per generation, and average generation to generation increments were -2.004×10^{-3}, -1.658×10^{-3}, and -1.61×10^{-4}. In each panel, large early downward steps were observed in the increment plots, followed by changes clustered near zero for the remainder of the run. The value histograms are dominated by counts at the lowest bin, and long plateaus near zero are visible in the trajectories. Taken together, these patterns indicate that the ν parameters were consistently driven toward irrelevance by optimization and were effectively pruned, which is consistent with the sparsity objective and with the aim of minimizing the number of active DVA parameters. A parameter-wise summary of convergence is presented in Table.3.

Table 3: Convergence summary for all tuned parameters over 500 generations.

Parameter	Initial	Final	Net Δ	Trend slope	Mean Δ/gen	Range	SD	Convergence outcome
$\boldsymbol{\beta_1}$	0.029003	0.015239	−0.013764	-6.0×10^{-6}	-2.8×10^{-5}	0.0307	0.0028	Stabilized interior; retained as a small active tuner
$\boldsymbol{\beta_7}$	0.591281	0.550909	−0.040372	-4.75×10^{-4}	-8.1×10^{-5}	0.3503	0.0712	Stabilized interior; major contributor
$\boldsymbol{\beta_8}$	0.771658	0.000106	−0.771553	-2.93×10^{-4}	-1.546×10^{-3}	0.7717	0.0621	Driven near zero; effectively pruned
$\boldsymbol{\lambda_1}$	0.772152	0.823493	+0.051342	-1.47×10^{-4}	$+1.03 \times 10^{-4}$	0.1695	0.0257	Stabilized interior; remained active
$\boldsymbol{\lambda_7}$	0.388707	0.257990	−0.130717	-4.43×10^{-4}	-2.62×10^{-4}	0.3565	0.0719	Stabilized interior; contributed without hitting bounds
$\boldsymbol{\lambda_8}$	0.948500	0.078876	−0.869625	-6.04×10^{-4}	-1.743×10^{-3}	0.9110	0.0993	Reduced to a small value; influence down-weighted
$\boldsymbol{\mu_1}$	0.393887	0.367100	−0.026756	-3.41×10^{-4}	-5.4×10^{-5}	0.2159	0.0535	Gradual decline and interior stabilization
$\boldsymbol{\nu_1}$	1.000000	0.000110	−0.999890	-1.72×10^{-4}	-2.004×10^{-3}	1.0000	0.0796	Collapsed to zero; pruned by sparsity
$\boldsymbol{\nu_7}$	0.827298	0.000013	−0.827285	-1.73×10^{-4}	-1.658×10^{-3}	0.9410	0.0896	Collapsed to zero; pruned by sparsity
$\boldsymbol{\nu_8}$	0.080362	0.000009	−0.080353	-2.28×10^{-4}	-1.61×10^{-4}	0.5171	0.0814	Collapsed to zero; pruned by sparsity

Conclusion

In this study, a unified and interpretable framework for dynamic vibration absorber (DVA) design was introduced to transform the shaping of frequency response functions (FRFs). Through the formulation of the singular criterion (C_s), a single, tunable measure was established to encode design intent, allowing target peak locations, amplitudes, and bandwidths to be specified directly, while unnecessary complexity was simultaneously penalized.

An adaptive genetic algorithm, implemented within the DeVana environment, was employed to optimize C_s across high-dimensional and nonconvex design spaces. When applied to a fully coupled 1DOF–1DOF benchmark with a 1000–2000 Hz avoidance band, the approach was shown to produce an absorber that effectively suppressed in-band responses, generated narrow edge peaks, and preserved baseline behavior outside the band. Convergence analyses confirmed consistent optimization and the automatic pruning of redundant parameters, resulting in a sparse yet effective configuration.

In practical terms, direct FRF shaping, built-in complexity control, and robust convergence were achieved without the need for manual tuning. Consequently, lighter, more interpretable, and less sensitivity-prone absorbers were obtained. In essence, DVA synthesis was reframed as a target-driven, automated process, in which desired FRF characteristics can be explicitly defined and minimal, physically meaningful solutions are automatically delivered. A practical foundation was thus established for efficient, adaptable, and experimentally viable absorber design.

Acknowledgement:

The authors would like to thank the reviewers for their valuable comments and their valuable insights in improving the quality of the paper. The authors would also like to thank the University of Kashan by providing the Grant No. 1392194/6.

Ethics Approval

The scientific content of this article is the result of the authors' research and has not been published in any Iranian or international journal.

Conflict of Interest

There are no other conflicts of interest to declare.

References

[1] H. Frahm, "Device for damping vibrations of bodies," ed: Google Patents, 1911.

[2] J. Ormondroyd and J. Den Hartog, "The theory of the dynamic vibration absorber," *Journal of Fluids Engineering,* vol. 49, no. 2, 1928. doi:10.1115/1.4058553

[3] J. P. Den Hartog, *Mechanical vibrations*. Courier Corporation, 1985.

[4] S. Randall, D. Halsted III, and D. Taylor, "Optimum vibration absorbers for linear damped systems," 1981. doi:10.1115/1.3255005

[5] G. B. Warburton, "Optimum absorber parameters for various combinations of response and excitation parameters," *Earthquake Engineering & Structural Dynamics,* vol. 10, no. 3, pp. 381-401, 1982. doi:10.1002/eqe.4290100304

[6] T. Gao, J. Li, S. Zhu, X. Yang, and H. Zhao, "H∞ Optimization of Three-Element-Type Dynamic Vibration Absorber with Inerter and Negative Stiffness Based on the Particle Swarm Algorithm," *Entropy,* vol. 25, no. 7, p. 1048, 2023. doi:10.3390/e25071048

[7] Y. Chen, H. Zhao, J. Zhang, H. Zhou, and H. Sun, "Optimization and Application of Particle Swarm Intelligence Algorithm in Maxwell Type Dynamic Vibration Absorber with Inerter Element," *Journal of Vibration Engineering & Technologies,* vol. 13, no. 5, p. 292, 2025. doi:10.1007/s42417-025-01869-8

[8] F. Zamani, S. H. Alavi, M. Mashayekhi, E. Noroozinejad Farsangi, A. Sadeghi-Movahhed, and A. Majdi, "Optimum design of double tuned mass dampers using multiple metaheuristic multi-objective optimization algorithms under seismic excitation," *Frontiers in Built Environment,* vol. 11, p. 1559530, 2025. doi:10.3389/fbuil.2025.1559530

[9] Y. Liu and L. Cheng, "Exact H∞ optimization of dynamic vibration absorbers: Univariate-polynomial-based algorithm and operability analysis," *Applied Mathematical Modelling,* vol. 139, p. 115812, 2025. doi:10.1016/j.apm.2024.115812

[10] A. Tollardo, F. Cadini, M. Giglio, and L. Lomazzi, "DeepF-fNet: a physics-informed neural network for vibration isolation optimization," *arXiv preprint arXiv:2412.21132,* 2024. doi: 10.48550/arXiv.2412.21132

[11] X. Chen, Y. Leng, F. Sun, X. Su, S. Sun, and J. Xu, "Design and modeling of a novel triple-magnet magnetic dynamic vibration absorber," *International Journal of Applied Electromagnetics and Mechanics,* vol. 71, no. 4, pp. 363-388, 2023. doi: 10.3233/JAE-220128

[12] J. Li, T. Gao, S. Zhu, and X. Yang, "H∞ optimization of a novel Maxwell dynamic vibration absorber with lever, inerter, and grounded stiffness," *Applied Sciences,* vol. 13, no. 6, p. 3697, 2023. doi:10.3390/app13063697

[13] Y. Peng and P. Sun, "Reliability-based design optimization of tuned mass-damper-inerter for mitigating structural vibration," *Journal of Sound and Vibration,* vol. 572, p. 118166, 2024. doi:10.1016/j.jsv.2023.118166

[14] Z.-Y. Xing and X.-D. Yang, "Parameter optimization of a two-stage quasi-zero-stiffness system with linear dynamic vibration absorber," *Nonlinear Dynamics,* vol. 112, no. 14, pp. 11887-11907, 2024. doi:10.1007/s11071-024-09704-7

[15] Y.-W. Chen, H.-T. Yau, T.-Y. Hsiao, S.-W. Hong, Y.-H. Cheng, and Y.-J. Wang, "Optimal Design using Particle Swarm Optimization for Ropeway Carrier Passive Dynamic Vibration Absorbers," in *2024 20th IEEE/ASME International Conference on Mechatronic and Embedded Systems and Applications (MESA)*, 2024: IEEE, pp. 1-7. DOI: 10.1109/MESA61532.2024.10704853

[16] F. A. Athifah and W. Hendrowati, "Experimental Analysis of Vibration Reduction of Boring Bar with Tapered Mass-Rubber Dynamic Vibration Absorber (MR-DVA)," *Engineering Proceedings,* vol. 84, no. 1, p. 65, 2025. doi:10.3390/engproc2025084065

[17] M. A. Shahraki, R. Kamgar, and H. Heidarzadeh, "Damage-based design of multiple tuned mass dampers to improve the seismic performance of steel frame structures," *Soil Dynamics and Earthquake Engineering,* vol. 173, p. 108062, 2023. doi:10.1016/j.soildyn.2023.108062

[18] B. Besharatian, H. T. Riahi, R. Garcia, and I. Hajirasouliha, "Particle swarm optimization of friction tuned mass dampers subjected to ground motion records," *Soil Dynamics and Earthquake Engineering,* vol. 172, p. 107995, 2023. doi:10.1016/j.soildyn.2023.107995

[19] S. Mazloom and A. K. Ghorbani-Tanha, "An Innovative Semiactive Rolling Tuned Mass Damper for Structural Vibration Mitigation," *Structural Control and Health Monitoring,* vol. 2025, no. 1, p. 9627790, 2025. doi.org/10.1155/stc/9627790

[20] M. Mousaviyan Safakhaneh, M. Fahimi Farzam, H. Ahmadi, and A. Farnam, "Vibration control of structure using active tuned mass damper: A new control algorithm," *Journal of Vibration and Control,* vol. 31, no. 13-14, pp. 2908-2919, 2025. doi:10.1177/10775463241263889

[21] S. Djerouni, G. Bekdaş, and S. M. Nigdeli, "Optimization and performance assessment of Multi-Tuned Mass Dampers (MTMD) to mitigate seismic pounding of adjacent buildings via a novel hybrid algorithm," *Journal of Building Engineering,* vol. 103, p. 112168, 2025. doi:10.1016/j.jobe.2025.112168

[22] Y. Luo, H. Sun, Z. Zhang, W. Wang, and L. Zuo, "Analytical optimization of the rotational inertia double tuned mass damper for structures under random excitation," in *Structures*, 2024, vol. 69: Elsevier, p. 107462. doi:10.1016/j.istruc.2024.107462

[23] F. Petrini, A. Giaralis, and Z. Wang, "Optimal tuned mass-damper-inerter (TMDI) design in wind-excited tall buildings for occupants' comfort serviceability performance and energy harvesting," *Engineering Structures,* vol. 204, p. 109904, 2020. doi:10.1016/j.engstruct.2019.109904

[24] F. A. Jabbar, P. S. Rao, and S. O. W. Khafaji, "Enhancing the Design of Dynamic Vibration Absorbers through Harmonic Analysis and Lumped Parallel Configuration," *Engineering, Technology & Applied Science Research,* vol. 14, no. 5, pp. 16624-16639, 10/09 2024, doi: 10.48084/etasr.7990. doi:10.48084/etasr.7990.

[25] A. Shamseldin, M. A. Abido, and A. Alofi, "AI-driven optimization of dynamic vibration absorbers with hydraulic amplifier and mechanical inerter integration," (in English), *Frontiers in Mechanical Engineering,* Original Research vol. Volume 10 - 2024, 2024-September-30 2024, doi: 10.3389/fmech.2024.1464692.

[26] V. D. Phuc and M.-T. Hoang, "A novel method for optimizing the parameters of dynamic vibration absorber for reducing torsional oscillations of high-speed rotor based on dual estimation," *Journal of Vibration and Control,* vol. 0, no. 0, p. 10775463251349876, doi: 10.1177/10775463251349876.

[27] *DeVana*. (2025). Github. [Online]. Available: https://github.com/mahan2079/DeVana

[28] T. Asami, O. Nishihara, and A. M. Baz, "Analytical solutions to H∞ and H 2 optimization of dynamic vibration absorbers attached to damped linear systems," *J. Vib. Acoust.,* vol. 124, no. 2, pp. 284-295, 2002.doi:10.1115/1.1456458.